# Organic & Biomolecular Chemistry

www.rsc.org/obc

Volume 11 | Number 44 | 28 November 2013 | Pages 7633–7804

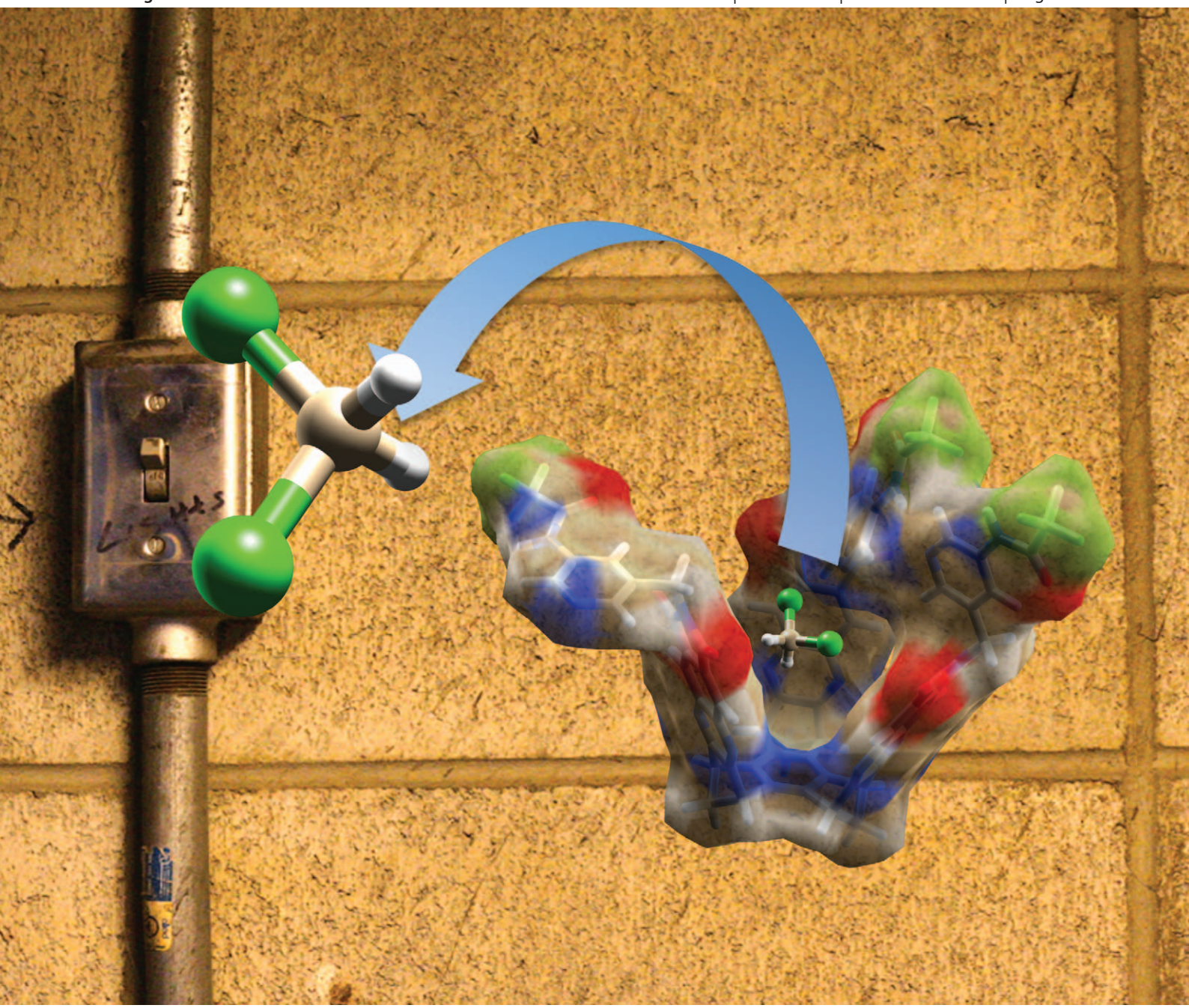

ISSN 1477-0520

RSC Publishing

**PAPER**

Jovica D. Badjić *et al.*

On the role of guests in enforcing the mechanism of action of gated baskets

Organic & Biomolecular Chemistry

RSC Publishing

PAPER

View Article Online
View Journal | View Issue



Cite this: *Org. Biomol. Chem.*, 2013, **11**, 7667

# On the role of guests in enforcing the mechanism of action of gated baskets†

Yian Ruan, Bao-Yu Wang, Jeremy M. Erb, Shigui Chen, Christopher M. Hadad and Jovica D. Badjić*

We designed and prepared a spacious and gated basket of type **2** ($V$ = 318 Å$^3$) in ten synthetic steps. With the assistance of $^1$H NMR spectroscopy, we found that the pyridine gates at the rim of **2** form a seam of N–H···N hydrogen bonds, thereby adopting right- (*P*) and left-handed (*M*) helical arrangements. The recognition characteristics of the smaller basket **1** ($V$ = 226 Å$^3$) and the larger **2** for various solvents as guests were quantified by $^1$H NMR spectroscopy in $CD_2Cl_2$ (61 Å$^3$), $CDCl_3$ (75 Å$^3$), $CFCl_3$ (81 Å$^3$) and $CCl_4$ (89 Å$^3$); the apparent guest binding equilibria $K_a$ were found to be inversely proportional to the affinity of bulk solvents $K_S$ for populating each host. The rate of the *P*/*M* racemization ($k_{rac}$, $s^{-1}$) was, for both **1** and **2**, studied in all four solvents using dynamic NMR spectroscopy. From these experiments, two isokinetic relationships ($\Delta S^{\ddagger}_{P/M}$ *vs.* $\Delta H^{\ddagger}_{P/M}$) were identified with each one corresponding to a different mechanism of *P*/*M* racemization. A computational study (B3LYP/6-31+G**//PM6) of **1** and **2** in the gas phase indicates two competing racemization pathways: (a) $RM_{1-2}$ describes a pivoting of a single gate followed by the rotation of the remaining two gates, while (b) $RM_3$ depicts simultaneous (geared) rotation of all three gates. The racemization of the larger basket **2**, in all four solvents (packing coefficient, PC = 0.19–0.28), conformed to one isokinetic relationship, which also coincided with the operation of the smaller basket **1** in $CD_2Cl_2$ (PC = 0.27). However, in $CDCl_3$, $CFCl_3$ and $CCl_4$ (PC = 0.33–0.39), the mode of action of **1** appears to correlate with a different isokinetic relationship. Thus, we propose that the population of the basket's inner space (PC) determines the mechanism of *P*/*M* racemization. When PC < 0.3, the mechanism of operation is $RM_{1-2}$, whereas, a greater packing, represented when PC > 0.3, enforces the geared $RM_3$ mechanistic alternative.

Received 7th July 2013,
Accepted 3rd September 2013

DOI: 10.1039/c3ob41511b

**www.rsc.org/obc**

## Introduction

A complete encirclement of guests by covalent/self-assembled hosts gives rise to encapsulation complexes.[1,2] A conformational change within the structure of the host,[3] of such complexes, could govern the in/out trafficking of guests,[4] and thus the encapsulation persistency ($\Delta G^{\ddagger}_{in/out}$).[5] For the entrapment to take place in the liquid phase, the size and shape of guests ought to be complementary[6] to the interior of the host.[7,8] Furthermore, ~55% population (packing coefficient, PC = $V_{guest}/V_{host}$)[9] of the cavitand's inner space[10] has been found to contribute to the formation of stable van der Waals encapsulation complexes.[11] The role of bulk solvent is important[12] as solvent molecules are in a constant quest to occupy the inner space of concave hosts while competing with other guests.[13] Markedly, sizeable molecules incapable of penetrating the capsular host and effectively solvating its concave surface[14] permit the formation of more stable encapsulation assemblies.[15] In fact, one could show (*vide infra*) that organic solvents capable of occupying the capsular host with an affinity of $K_S > 10^{-2}$–$10^{-3}$ $M^{-1}$ weaken the binding to the point that there is almost no measurable complexation.[16] In a similar manner, polar water molecules are incompatible with the interior of hydrophobic organic hosts, thereby assisting guest complexation *via* the hydrophobic effect.[19,20] Evidently, the effective formation of encapsulation complexes[21] is a function of the solvophobic effect,[22] yet finding a suitable medium for exploring encapsulation is still a matter of experimental investigation.[23]

Our mechanistic studies of gated baskets of type **1** (226 A$^3$, Fig. 1A) have, so far, been completed in dichloromethane ($CD_2Cl_2$, 61 Å$^3$), and the affinity for guests was satisfactory.[24] Accordingly, in this environment, the basket can be classified as solvophobic: one $CD_2Cl_2$ (61 A$^3$, PC = 28%) is not enough to populate its cavity, two $CD_2Cl_2$ are not complementary to the

*Department of Chemistry and Biochemistry, 100 West 18th Avenue, Columbus, Ohio, USA. E-mail: badjic@chemistry.ohio-state.edu; Fax: +614-292-1685; Tel: +614-247-8342*

†Electronic supplementary information (ESI) available: Additional experimental/computational results and spectra for new compounds. See DOI: 10.1039/c3ob41511b

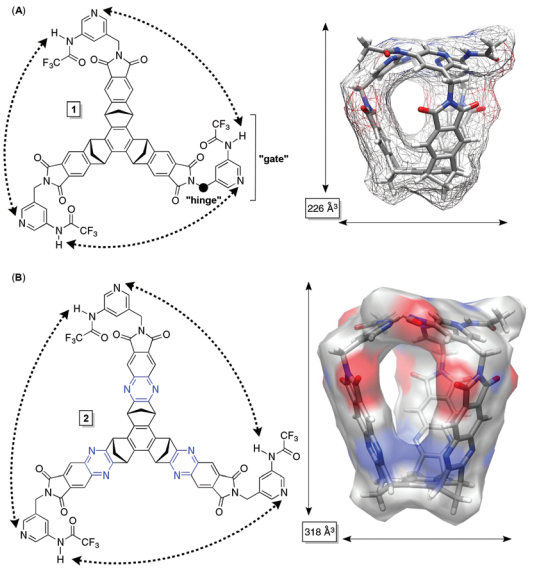


**Fig. 1** Chemical structures of basket **1** (A) and **2** (B) forming intramolecular N–H···N hydrogen bonds and their corresponding energy-minimized forms (PM6). The volume of each basket's cavity was computed by the 3 V computational method[17] while their van der Waals surfaces are visualised using UCSF Chimera software.

inner concave surface (122 Å$^3$, PC = 55%), while three $CD_2Cl_2$ are simply too much for occupying the interior (183 Å$^3$, PC = 83%); note that dissolved gases ($N_2$, $O_2$, Ar, *etc.*)[25] could potentially fill the cavity of cavitands as well.[26] Importantly, numerous haloalkanes (~80–125 Å$^3$)[27] were found to substitute weakly bound solvent within **1** in a process that is first-order in both guest and basket ($v_{in} = k_{in}$ [basket] [guest]).[28] The recognition is driven by enthalpy ($\Delta H^\circ < 0$)[27] while the entropic contributions are adverse in most cases ($\Delta S^\circ < 0$).[5] In this basket, the three hydrogen-bonded pyridines (gates) revolve at the rim adopting right- (*P*) and left-handed (*M*) orientations.[29] The rotation creates a sizeable aperture at the basket's northern side to permit the solvent/guest exchange.[30] Regulation of the dynamics of the fluctuating entrance is important for controlling the chemoselectivity[29,31] by which molecules access the basket's cavity as well as the lifetime of encapsulation complexes.[32] Importantly, the hydrogen-bonded gates could rotate without guest species entering/departing the basket's inner space.[30] Will a more sizeable basket **2** (318 A$^3$, Fig. 1B) also form a gated host? How will a bigger cavity affect the mechanism of in/out guest exchange? Does the *P*/*M* racemization mechanism in any way relate to the size of the basket's interior? Does the guest size have any effect on the mechanism by which baskets operate? To address these questions, we used methods of both experimental and computational chemistry and examined the inner solvation, conformational dynamics, and encapsulation characteristics of **1** and **2**. Interestingly, it appears that the filling of the basket's cavity determines the mechanism by which each gated host opens and closes its gates to control the encapsulation kinetics.

## Results and discussions

### Design and preparation of basket 2

To make a bigger gated host, one could extend the phthalimide groups in basket **1** (Fig. 1A) by incorporating quinoxaline moieties into the tris-norbornane framework (Fig. 1B).[18] Indeed, we already optimized a template-directed protocol for the preparation of bowl-shaped $\mathbf{4}_{syn}$ (Fig. 2A).[18] In accord with this methodology, compound **3** was cyclotrimerized to give *syn* diastereomer of **4** with Cu(I)/Cs(I) as templating cations and Pd(0)/Cu(I) as catalysts (Fig. 2A). The synthetic strategy could therefore be useful for the preparation of more spacious basket **2** (Fig. 1B), although we had to experimentally test the cyclotrimerization of **9** under the same or a similar set of conditions (Fig. 2B).[18] Dimethyl-4,5-diaminophthalate **5** (Fig. 2B) was obtained in gram quantities following already reported procedures (Scheme S1†).[35,36] The condensation of this compound with 5-norbornene-2,3-dione **6** ($CH_2Cl_2$) was facile and provided **7** in 92% yield. The bromination/dehydrobromination of **7** gave bromoalkene **8** (60%), which was further stannylated at low temperature (195 K) to form compound **9** (Fig. 2B). The cyclotrimerization of bromo(trimethylstannyl) **9** was attempted with a Pd(0)/Cu(I)/CsF catalytic system (Table S1†). As discussed earlier, Cu(I)/Cs(I) metal cations were expected[18] to template the formation of $\mathbf{10}_{syn}$ by coordinating to quinoxaline nitrogen atoms within the basket's framework. Interestingly, diastereomeric $\mathbf{10}_{syn}$ and $\mathbf{10}_{anti}$ were obtained in a nearly statistical ratio (~1 : 3) and overall 60% yield. Given the absence of templation, the reaction's outcome is attributed to both electronic and steric factors: (1) less basic quinoxaline nitrogen atoms in **9**, carrying two electron-withdrawing ester functionalities, ought to have a lower coordination affinity toward metal cations, and (2) six ester groups at the rim of $\mathbf{10}_{syn}$ could hinder the formation of a more compact transition state that is required for its formation. The base-catalyzed (LiOH) hydrolysis of hexamethylester $\mathbf{10}_{syn}$ followed by treatment of the hexaacid with trifluoroacetic anhydride (TFAA, Fig. 2B) gave tris-anhydride **11**. The conjugation of diamine **12** to **11** gave tris-amine **13**, which upon condensation with TFAA afforded basket **2** in 41% yield.

### NMR characterization of basket 2

$^1$H NMR spectrum of basket **2** (400 MHz, $CDCl_3$) showed a set of signals corresponding to a $C_{3v}$ symmetric molecule (Fig. 3A); $^1$H–$^1$H NOESY spectroscopic correlations (Fig. S1†) allowed us to assign all of the basket's resonances. Notably, the singlet corresponding to the three amide N–H protons is positioned downfield ($\delta$ = 11.9 ppm, Fig. 2C), confirming the formation of N–H···N hydrogen bonds. In fact, a dilution of $CDCl_3$ solution of **2** (from 0.8 to 0.1 mM, Fig. S2†) caused a negligible shift of the N–H resonance to indicate the absence of intermolecular aggregation. In line with this result, NMR diffusion measurements (2D DOSY, 298.0 K) of 0.8–0.3 mM solution of **2** in $CDCl_3$ showed a set of signals with similar diffusion coefficients ($D$ = 5.4–7.4 × 10$^{-10}$ m$^2$ s$^{-1}$, Fig. S3†); the computed Stokes–Einstein radius $R_H$ = 5.4–7.5 Å of **2** bodes

 

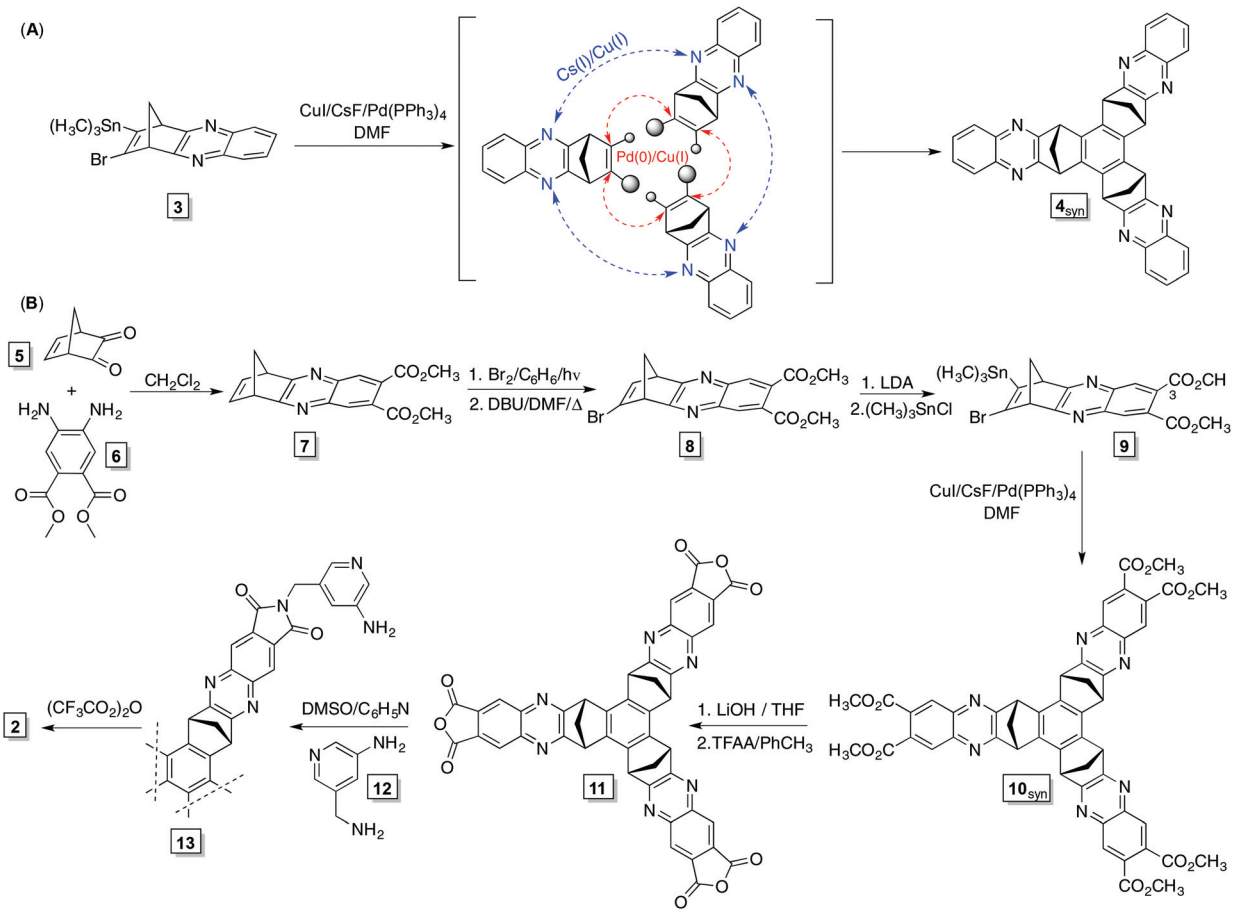


**Fig. 2** (A) Template-directed synthesis of cup-shaped $\mathbf{4}_{syn}$ as reported previously.[18] (B) The preparation of basket **2** was completed in ten synthetic steps.

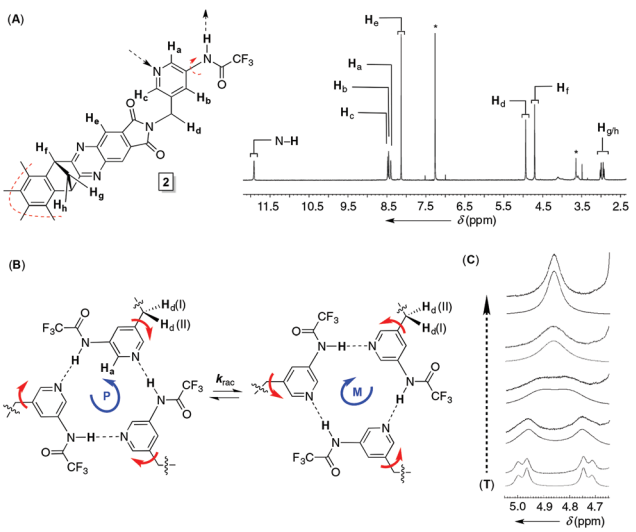


**Fig. 3** (A) Chemical structure of basket **2** and $^1$H NMR spectrum (400 MHz) of this compound (298.0 K) in $CDCl_3$. (B) Pyridine gates in **2** adopt *P* and *M* stereochemical arrangements with rate coefficient $k_{rac}$ characterizing the $\mathbf{2}_{P/M}$ interconversion. (C) A segment of simulated (bottom, WinDNMR)[33,34] and experimental (top) VT $^1$H NMR spectra of basket **2** in $CD_2Cl_2$ showing the coalescence of an AB quartet, corresponding to $\mathbf{H}_d$ protons, into a singlet.

well with the approximate diameter (12–15 Å, Fig. 1) of this basket. In conclusion, host **2** is monomeric in $CDCl_3$ with pyridine gates forming intramolecular N–H···N contacts.

Despite a slightly greater distance between the "hinge" $CH_2$ groups at the rim of **2** with respect to **1** ($\Delta d$ = 0.5 Å, Fig. 1), the pyridine gates are apparently close enough to make non-covalent contacts: for both baskets, the N–H···N distances are almost identical, 3.13–3.16 Å, while the corresponding bond angles are somewhat different (148–154°, Fig. 1). Importantly, a comparison of the computed structural parameters for **1** and **2** also shows a small contraction of the cup-shaped platform of **2** to perhaps assist the formation of the N–H···N contacts.

## The inner space of baskets 1 and 2

Assessing the volume enclosed by the van der Waals surface of a concave host is a challenging task,[37,38] as one has to account for the host's corners/dimples as well as arbitrate on the molecule's boundary surface.[10] A rapid computational method for completing this job would certainly be useful to experimentalists as the encapsulation selectivity is a function of the population of the host's cavity.[10] That is to say, stable van der Waals encapsulation complexes are typically obtained when PC =

0.55 ± 0.09, which is in the range of the packing density of common organic liquids (PC = 0.51–0.63).[10]

The optimal distance between neutral atoms forming a stable noncovalent complex is, from a Lennard-Jones potential curve, 1.12 times greater ($r_e = 2^{1/6}\sigma$; $-dU/dr$ = Force = 0)[39] than the sum of their van der Waals radii.[8] Given such an analysis, envision a system of two atoms as spheres, each having 1 Å radius and at the necessary equilibrium distance of $r_e$ = 2.24 Å. If the radius of the first sphere is kept constant ($r_1$ = 1 Å) while that of the second is increased to $r_2$ = 1.24 Å, then we can enclose the smaller into the bigger sphere to efficiently populate the space. Next, we can calculate that the volume occupied by the smaller sphere ($V_1/V_2 = (r_1/r_2)^3$) amounts to 52%, which is within the range of reported packing coefficient of liquids![10]

To compute the inner space of baskets **1** and **2** (Fig. 1), we used the recently developed 3 V (Voss Volume Voxelator) computational protocol;[17] this freeware has been recommended for investigating drug-binding sites in biological molecules and is readily available at http://3vee.molmovdb.org. In essence, the method employs two variously sized rolling probes elucidating the shape of the molecule of interest: the bigger probe (typically $r_1$ > 10 Å) must not populate the cavity to establish the outer molecular surface, while the smaller probe (depending on its size) delineates the accessible ($r_2$ > 0) or van der Waals ($r_2$ = 0) surface of the molecule. The subtraction of two computed surfaces, comprising a 3D grid of 0.5 Å voxels, gives the volume.

The distance between two carbonyl oxygen atoms across the aperture of energy-minimized **1** and **2** (MMFFs, Spartan) is ~6.2–6.8 Å and the 10 Å ($r_1$) virtual probe shall not penetrate the cavity. The size of the smaller probe ($r_2$ = 0.2 Å), however, was chosen to obtain the volume of the smaller basket **1** (226 Å$^3$) close to the value calculated with the cavity filling method (221 ± 9 Å$^3$).[27] Following this same protocol (with $r_1$ = 10 Å and $r_2$ = 0.2 Å), the cavity of the larger basket **2** was estimated to be 318 Å$^3$ (Fig. 1B). Importantly, varying the radius of the bigger probe ($r_1$ = 9–11 Å) had a small effect on the computed volumes (±2%). The variation of the smaller probe ($r_2$ = 0.1–0.3 Å), however, had a greater effect on the volume variation (±9%). To further assess the utility of this rapid methodology for determining the volume of artificial cavitands, we examined the inner space of eight variously sized/shaped capsular hosts (Table 1). Importantly, the computed 3 V volume of these molecules is comparable to the values obtained from the cavity-filling method (Table 1).[10]

**Table 1** The inner volume of various molecular capsules computed with the 3 V and cavity-filling methods

| Capsule | 3 V method[17] (Å$^3$) | Cavity-filling method[10] (Å$^3$) | Variation (%) |
|---|---|---|---|
| Tennis ball I[40] | 50 | 52 | −4 |
| Tennis ball II[41] | 83 | 68 | 18 |
| Softball[42] | 362 | 322 | 11 |
| Cryptophane A[16] | 114 | 97 | 15 |
| Calix[4]arene dimer[38] | 205 | 197 | 4 |
| Calix[4]arene carceplex[43] | 161 | 159 | 1 |
| Carceplex[44] | 127 | 117 | 8 |
| Cylindrical capsule[45] | 423 | 420 | 1 |

$$[\mathbf{G}] + [\mathbf{B}]_{free} \overset{K}{\rightleftharpoons} [\mathbf{G}{<}\mathbf{B}]$$
$$+$$
$$[\mathbf{S}] \overset{K_S}{\rightleftharpoons} [\mathbf{S}{<}\mathbf{B}]$$

**Scheme 1**

### On the encapsulation thermodynamics

Numerous solvent molecules surround a concave host with a tendency to occupy its interior.[45] Thus, bulk solvent [**S**] could act as guest[14] and reside in the cavity of unoccupied molecular capsules $[\mathbf{B}]_{free}$ to give the [**S**⊂**B**] complex ($K_S$, Scheme 1). The greater the stability of the [**S**⊂**B**] complex ($K_S$), the lower the concentration of the desired host–guest complex [**G**⊂**B**] ($K$, Scheme 1). In essence, two competing equilibria determine the outcome of the recognition process and thereby the formation of [**G**⊂**B**]. It follows that solvents with a greater affinity $K_S$ ($M^{-1}$) for residing in the host are also more competitive. That is, solvent molecules can reduce the experimentally measured and apparent affinity $K_a$ (eqn (1)) of a guest [**G**] occupying the host in its free and solvated forms ($[\mathbf{B}]' = ([\mathbf{B}]_{free} + [\mathbf{S}\subset\mathbf{B}])$. The apparent affinity $K_a$ is, therefore, given as:

$$[\mathbf{G}] + [\mathbf{B}]' = [\mathbf{G}\subset\mathbf{B}]$$

$$K_a = [\mathbf{G}\subset\mathbf{B}]/([\mathbf{G}][\mathbf{B}]')$$

$$[\mathbf{B}]' = ([\mathbf{B}]_{free} + [\mathbf{S}\subset\mathbf{B}]) \quad (1)$$

From Scheme 1, one can derive:

$$K = [\mathbf{G}\subset\mathbf{B}]/([\mathbf{G}][\mathbf{B}]_{free}) \quad (2)$$

$$K_S = [\mathbf{S}\subset\mathbf{B}]/([\mathbf{S}][\mathbf{B}]_{free}) \quad (3)$$

By dividing eqn (1) and (2), we obtain:

$$K_a/K = [\mathbf{B}]_{free}/[\mathbf{B}]'$$

$$K_a/K = [\mathbf{B}]_{free}/([\mathbf{B}]_{free} + [\mathbf{S}\subset\mathbf{B}]) \quad (4)$$

From eqn (3) into (4), however, it follows:

$$[\mathbf{S}\subset\mathbf{B}] = K_S[\mathbf{S}][\mathbf{B}]_{free}$$

$$K_a/K = [\mathbf{B}]_{free}/([\mathbf{B}]_{free} + K_S[\mathbf{S}][\mathbf{B}]_{free}$$

$$K_a/K = 1/(1 + K_s[\mathbf{S}]) \quad (5)$$

Finally, the relationship between three stability constants[16] is obtained:

$$K_a = K/(1 + K_s[\mathbf{S}]) \quad (6)$$

The concentration of organic solvents is typically in the range of [**S**] = 10–15 $M^{-1}$, and if $K_S$ < 0.01 $M^{-1}$, then eqn (6) reduces to $K_a \sim K$: the apparent affinity $K_a$ of the basket for trapping the targeted guest is close to the intrinsic affinity $K$ and is hardly affected by the solvent. However, when the

 

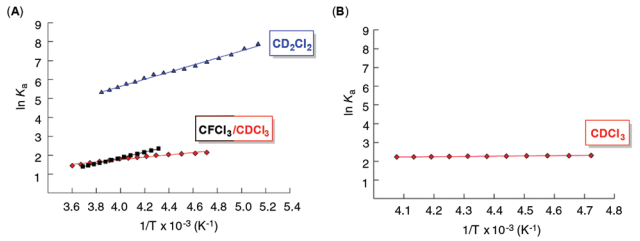


**Fig. 4** (A) The apparent binding affinity $K_a$ ($M^{-1}$) of $(CH_3)_2CBr_2$ for occupying basket **1** was measured (VT $^1$H NMR, Fig. S4–S7†) in four different solvents. (B) The apparent binding affinity $K_a$ ($M^{-1}$) of $C_2Cl_6$ for occupying basket **2** was quantified (VT $^1$H NMR, Fig. S8–S11†) in $CDCl_3$, while it was below the detection limit in $CD_2Cl_2$, $CFCl_3$ and $CCl_4$.

affinity of solvent molecules for occupying the basket is greater ($K_S$ > 0.1 $M^{-1}$), then the apparent binding $K_a$ decreases and eqn (6) gives $K_a \leq K/2$.

We used VT $^1$H NMR spectroscopy to measure the apparent affinity $K_a$ of 2,2-dibromopropane (107 Å$^3$, PC = 0.47) towards basket **1** (226 Å$^3$) in four differently sized solvents: $CD_2Cl_2$, 61 Å$^3$; $CDCl_3$, 75 Å$^3$; $CFCl_3$, 81 Å$^3$ and $CCl_4$, 89 Å$^3$ (Fig. 4A).[27] On the basis of size, these solvents were expected to fill the basket's interior (PC = 0.27–0.39, Table 2) with an increasingly greater affinity $K_s$ for occupying its cavity along the series. Indeed, the stability of $[(CH_3)_2CBr_2\subset\mathbf{1}]$ was found to be greater in $CD_2Cl_2$ (ln $K_a$ > 5.3, Fig. 4A) than in $CDCl_3$/$CFCl_3$ (ln $K_a$ < 2.3, Fig. 4A) while practically non-measurable in $CCl_4$. From eqn (6), we can deduce the following trend: $K_s^{CD2Cl2} < K_s^{CDCl3/CFCl3} < K_s^{CCl4}$. Since $K_a^{CD2Cl2}$ is ~$10^2$–$10^3$ $M^{-1}$ ($K > 10^2$ $M^{-1}$), it is reasonable to assume $K_s^{CCl4}$ to be >10 $M^{-1}$ for shutting off the encapsulation ($K_a^{CCl4} < 1$) in this environment.

The apparent affinity $K_a$ of basket **2** (318 Å$^3$) toward hexachloroethane $C_2Cl_6$ (137 Å$^3$, PC = 0.43) was, as in the case above, measured with $^1$H NMR spectroscopy in four differently sized solvents (Fig. 4B). Markedly, the binding affinity could be quantified in $CDCl_3$ while it is difficult to measure (too weak) in $CD_2Cl_2$, $CFCl_3$, and $CCl_4$. For the more sizeable basket **2**, there is a smaller affinity for chloroform than the remaining three solvents for occupying the cavity. The basket can therefore be characterized as solvophobic in $CDCl_3$ ($K_s^{CDCl3} < K_s^{CD2Cl2/CFCl3/CCl4}$); we realize that for future recognition studies, we need to survey other solvents.

## Axial *P*/*M* chirality in gated baskets

Previously, we found that the formation of N–H···N hydrogen bonds at the northern portion of basket **1** would limit the torsional motion about each of its three C–NH(C═O) single bonds (Fig. 2B).[24] In accord with this conformational bias, we measured NOE magnetization transfer (298.0 K, Fig. S1†) between resonances corresponding to N–**H** and $\mathbf{H}_a$ protons in the larger basket **2** (Fig. 2B). It follows that the pyridine gates in **2** are also adopting right- (*P*) and/or left-handed (*M*) orientations[29] with a pair of diastereotopic $\mathbf{H}_d$ hydrogen atoms at the "hinge" (Fig. 3B). Indeed, variable temperature $^1$H NMR spectra (400 MHz, $CDCl_3$) of **2** supported the existence of *P*/*M* stereoisomers: a singlet corresponding to $\mathbf{H}_d$ protons at higher temperatures would change into an AB quartet at lower temperatures (Fig. 3C). The classical band-shape analysis (WinDNMR)[33,34] of the NMR spectroscopic data provided rate coefficient $k_{rac}$ (Fig. 3B) characterizing the rotation of the gates and thereby the racemization of $\mathbf{2}_{P/M}$ in $CDCl_3$. Importantly, we completed a series of VT-NMR measurements for baskets **1** and **2** in four differently sized solvents: $CD_2Cl_2$, 61 Å$^3$; $CDCl_3$, 75 Å$^3$; $CFCl_3$, 81 Å$^3$ and $CCl_4$, 89 Å$^3$. The activation parameters $\Delta H^{\ddagger}_{P/M}$ and $\Delta S^{\ddagger}_{P/M}$ (Table 2), characterizing the racemization, were extracted from the corresponding Eyring plots (Fig. S12–19†).

## The revolving of pyridine gates and the inner solvation of baskets

The revolving of pyridine gates is, in both baskets **1** and **2**, characterized with negative entropy of activation for all four solvents ($\Delta S^{\ddagger}_{P/M}$ = −6 to −23 e.u., Table 2). Thus, in the mechanism for the *P*/*M* conversion (*vide infra*), the seam of N–H···N hydrogen bonds must loosen up and break in the rate-controlling step of the transformation (Fig. 3B). This, in turn, should augment the framework's flexibility contributing to its greater disorder ($\Delta S^{\ddagger}_1 > 0$, Scheme 2). Concurrently, the same unfolding of the basket's framework contributes to the extension of its surface area to prompt a more excessive solvation. Additional solvent molecules ought to surround the partly open capsular host and interact with it, to presumably increase the order of the system ($\Delta S^{\ddagger}_2 < 0$, Scheme 2). To explain the experimental result (Table 2), the adverse entropy of solvation

**Table 2** The interconversion of $\mathbf{1}_{P/M}$ and $\mathbf{2}_{P/M}$ stereoisomers is, in four differently sized solvents, characterized with $\Delta H^{\ddagger}_{P/M}/\Delta S^{\ddagger}_{P/M}$ activation parameters (Fig. S12–19). Packing coefficients were computed for one solvent molecule occupying each basket's interior. Note that it is difficult to computationally (MMFFs) fit more than one solvent molecule in the interior of each basket without breaking the seam of hydrogen bonds at the northern side

| | Basket **1** (226 Å$^3$) | | | | Basket **2** (318 Å$^3$) | | | |
|---|---|---|---|---|---|---|---|---|
| Parameters | $CD_2Cl_2$ | $CDCl_3$ | $CFCl_3$ | $CCl_4$ | $CD_2Cl_2$ | $CDCl_3$ | $CFCl_3$ | $CCl_4$ |
| $\Delta H^{\ddagger}_{P/M}$ (kcal mol$^{-1}$) | 8.98 ± 0.19 | 9.90 ± 0.14 | 7.30 ± 0.10 | 7.97 ± 0.15 | 6.40 ± 0.12 | 7.75 ± 0.13 | 4.60 ± 0.10 | 6.82 ± 0.07 |
| $\Delta S^{\ddagger}_{P/M}$ (e.u.) | −6.61 ± 0.85 | −7.80 ± 0.57 | −18.45 ± 0.42 | −16.32 ± 0.61 | −16.82 ± 0.56 | −11.14 ± 0.62 | −23.49 ± 0.50 | −14.50 ± 0.36 |
| Volume (Å$^3$) | 61 | 75 | 81 | 89 | 61 | 75 | 81 | 89 |
| Packing coefficient (PC) | 0.27 | 0.33 | 0.36 | 0.39 | 0.19 | 0.24 | 0.25 | 0.28 |

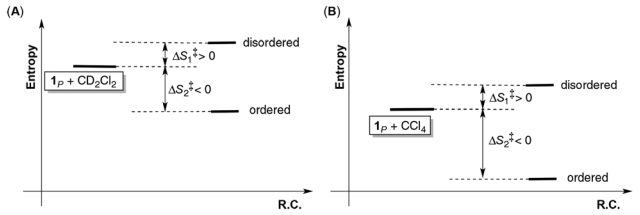


**Scheme 2** The entropy of activation $\Delta S^{\ddagger}_{P/M}$ of basket **1** (A: $CD_2Cl_2$; B: $CCl_4$) is partitioned into more favourable $\Delta S^{\ddagger}_1$, pertaining to the flexibility of the molecular framework, and adverse $\Delta S^{\ddagger}_2$, describing the solvation changes.

must be dominant in the course of the *P*/*M* change: $\Delta S^{\ddagger}_{P/M} = \Delta S^{\ddagger}_1 + \Delta S^{\ddagger}_2$ with $|\Delta S^{\ddagger}_2| > |\Delta S^{\ddagger}_1|$.

The entropy of activation, characterizing $\mathbf{1}_{P/M}$ interconversion, is "smaller" for $CD_2Cl_2$ ($\Delta S^{\ddagger}_{P/M} = -6.61 \pm 0.85$ e.u.) than any other solvent (Table 2). We surmise that host **1** undergoes a less dramatic solvation change in $CD_2Cl_2$ (smaller $|\Delta S^{\ddagger}_2|$ term, Scheme 1A) as turning into the corresponding transition state, in the course of the *P*/*M* interconversion. The greater entropic change in $CCl_4$ ($\Delta S^{\ddagger}_{P/M} = \updownarrow 16.32 \pm 0.61$ e.u., Table 2), however, suggests a more significant solvent reorganization (with a bigger $|\Delta S^{\ddagger}_2|$ term, Scheme 1B) along the *P*/*M* transition. As discussed earlier, basket **1** is solvophobic in $CD_2Cl_2$ and solvophilic in $CCl_4$ ($K_s^{CCl4} \gg K_s^{CD2Cl2}$, Fig. 4A). Accordingly, $CCl_4$ solvent molecules are more attracted to the interior of $\mathbf{1}_{P/M}$ to contribute to a more ordered ground state (Scheme 2B). This, in turn, renders a greater solvation change during the racemization (Scheme 2B). In the case of $\mathbf{1}_{P/M}$ conversion in $CD_2Cl_2$, however, the ground state of **1** is poorly solvated (*i.e.* more disordered) and a smaller change in its order is necessary to reach the transition state.

The activation entropy for $\mathbf{2}_{P/M}$ interconversion is most favourable in $CDCl_3$ ($\Delta S^{\ddagger}_{P/M} = -11.14 \pm 0.62$ e.u., Table 2). It follows that the basket should be more solvophobic in this medium with a poorly solvated ground state. This is in agreement with our encapsulation studies in which $CDCl_3$ is indeed the least competitive solvent with $K_s^{CDCl3} < K_s^{CD2Cl2/CCl4/CFCl3}$ (Fig. 4B).

## The mechanism of *P*/*M* racemization – computational study

For the racemization of the $C_3$ symmetric basket **1**, we considered two mechanistic alternatives $RM_{1-2}$ and $RM_3$ (Fig. 5).[46–48] In the one/two-gate $RM_{1-2}$ transformation (Fig. 5A), the racemization begins with one pyridine gate "breaking away" from the N–H···N hydrogen bonding in **1** to form an intermediate state. The concomitant flip of the remaining two gates completes the *P*/*M* conformational interconversion; note that this particular mechanism is reminiscent of Mislow's two-ring flip within molecular propellers.[46] However, for the three-gate $RM_3$ racemization (Fig. 5B), all three gates undergo a synchronized revolving motion that reverses the basket's helicity in one elementary step.[49] In our prior work, we examined the departure of $CBr_4$ from gated baskets of type **1** using steered molecular dynamics (SMD).[28] The cleavage of all three intramolecular N–H···N hydrogen bonds would, in this particular case, take place with the departure of $CBr_4$ (108 Å$^3$, PC = 0.48) from the basket. Given the interdependence between the rotation of the gates and the in/out guest exchange,[24,30,32] we deduced that the three-gate $RM_3$ mechanism dominates in the case of the **1**/$CBr_4$ system.

In line with the above considerations, we completed a series of dihedral-driver computations of baskets **1** and **2** (PM6 for geometries, followed by B3LYP/6-31+G** single-point energies) containing both methyl (R = $CH_3$, Table 3) and trifluoromethyl (R = $CF_3$, Table 3) amide groups and undergoing two racemisation pathways, $RM_{1-2}$ and $RM_3$ (Fig. 5). Importantly, for all of these calculations, the baskets were empty (*i.e.*, no guest), and calculations were performed in the gas phase. For the $RM_{1-2}$ process, we drove the rotation of one pyridine gate by constraining its O=C–N–C dihedral angle, $\varphi_1$. Specifically, the rotation of the pyridine gate from the inner to the outer side of the basket was evaluated in 5° increments; upon each change in $\varphi_1$, the structure was subjected to energy minimization and the overall energy was computed. To complete the inversion of chirality, we drove the rotation of the remaining two gates by restricting their dihedral angle $\varphi_2$ (Fig. 5A). The

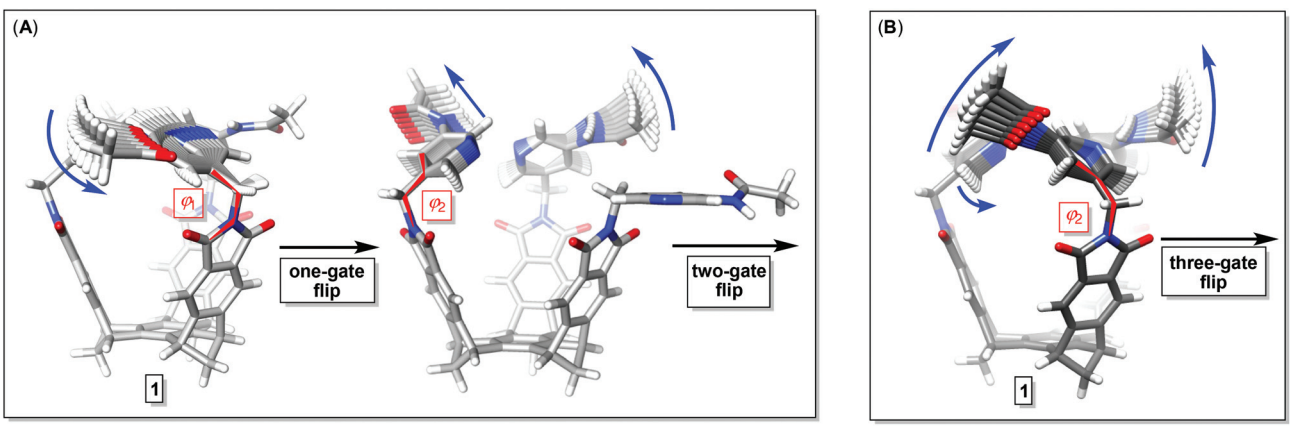


**Fig. 5** (A) One/two-gate racemization mechanism ($RM_{1-2}$) of **1** was computed (B3LYP/6-31+G**//PM6) to proceed *via* rotation of one gate ($\varphi_1$) followed by simultaneous rotation of the remaining two gates ($\varphi_2$). (B) Three-gate racemization mechanism ($RM_3$) of **1** was computed (B3LYP/6-31+G**//PM6) to proceed *via* simultaneous rotation of all three gates ($\varphi_2$).

 

**Table 3** The activation energy difference ($\Delta E$, kcal mol$^{-1}$) between two racemization pathways, $RM_{1-2}$ and $RM_3$ (see text), was computed for the interconversion of $\mathbf{1}_{P/M}$ and $\mathbf{2}_{P/M}$ stereoisomers at the PM6//PM6 and B3LYP/6-31+G**//PM6 levels of theory

| | PM6//PM6 | | B3LYP/6-31+G**//PM6 | |
|---|---|---|---|---|
| Basket $\mathbf{1}_R/\mathbf{2}_R$ | Preferred mechanism | $\Delta E$ (kcal mol$^{-1}$) | Preferred mechanism | $\Delta E$ (kcal mol$^{-1}$) |
| $\mathbf{1}_{CH3}$ | $RM_{1-2}$ | 4.3 | $RM_{1-2}$ | 0.2 |
| $\mathbf{2}_{CH3}$ | $RM_{1-2}$ | 1.3 | $RM_{1-2}$ | 5.6 |
| $\mathbf{1}_{CF3}$ | $RM_{1-2}$ | 0.1 | $RM_3$ | 4.7 |
| $\mathbf{2}_{CF3}$ | $RM_3$ | 0.7 | $RM_3$ | 9.8 |

potential energy landscape of the three-gate mechanism $RM_3$ was examined by simultaneous variation of all three dihedral angles $\varphi_2$ (Fig. 5B). The computed difference of activation energies ($\Delta E$) for two mechanistic alternatives is summarized in Table 3.

Energies from the PM6 optimizations predict that both (empty) acetamide baskets ($\mathbf{1}_{CH3}$, $\mathbf{2}_{CH3}$) would prefer the $RM_{1-2}$ mechanism. The same preference for $RM_{1-2}$ exists for single-point energies at the B3LYP/6-31+G** level of theory, although the stronger preference for $RM_{1-2}$ is with $\mathbf{2}_{CH3}$ instead of $\mathbf{1}_{CH3}$. The PM6 optimizations of $\mathbf{1}_{CF3}$ showed a slight preference (~0.1 kcal mol$^{-1}$) for $RM_{1-2}$, while those done with $\mathbf{2}_{CF3}$ support the $RM_3$ pathway. It is important to remember that the experimental results with different solvents were obtained for the $CF_3$ baskets of **1** and **2**. Single-point energy calculations on $\mathbf{1}_{CF3}$ and $\mathbf{2}_{CF3}$ point to $RM_3$ as the preferred mechanism (Table 3). Importantly, these calculations were completed in the gas phase, and without consideration of any solvent in the cavity; indeed, the inclusion of a guest and solvation could alter the behavior of the baskets. Given such considerations, we conclude that our computational data suggest two competing pathways with comparable energies of activation.

### The mechanism of the *P*/*M* racemization – experimental study

The free energy of activation $\Delta G^{\ddagger}_{P/M}$ ($\Delta G^{\ddagger}_{P/M} = \Delta H^{\ddagger}_{P/M} - T\Delta S^{\ddagger}_{P/M}$, Table 2) for the *P*/*M* racemization of baskets **1** and **2** is plotted over the 180–340 K temperature range (Fig. 6A/B). Interestingly, the opening/closing of the smaller basket **1** is fastest in $CD_2Cl_2$ (Fig. 6A) relative to the other three solvents ($\Delta G^{\ddagger}_{P/M}$ < 11 kcal mol$^{-1}$, Fig. 6A). The nature of bulk solvent had, however, a less dramatic effect on the dynamics of basket **2** (Fig. 6B). The interconversion rate of $\mathbf{2}_{P/M}$ is similar in all four environments but also akin to basket **1** in $CD_2Cl_2$ (Fig. 6A)! Another way to present the data in Fig. 6A/B is by plotting the interdependence between enthalpy $\Delta H^{\ddagger}_{P/M}$ and entropy $\Delta S^{\ddagger}_{P/M}$ characterizing the racemization (Fig. 6C).[50] Evidently, there are two isokinetic relationships[51] with similar isokinetic temperatures $\beta = (\Delta H^{\ddagger}_{P/M} - \Delta H^{\ddagger}_{o})/\Delta S^{\ddagger}_{P/M}$ = 240–260 K. In essence, the *P*/*M* racemization of (a) basket **1** in $CDCl_3$, $CFCl_3$ and $CCl_4$ appears to follow one mechanism while (b) basket **2** in all four solvents another mechanism, which as well operates for **1** in $CD_2Cl_2$ (Fig. 6C).[51,52]

In line with this interpretation, we observe that the size of the solvent molecules should matter in opening/closing of gated baskets by imposing on the operation of gates rotating at the rim. That is to say, the enthalpic component $\Delta H^{\ddagger}_{P/M}$ of the racemization energy $\Delta G^{\ddagger}_{P/M}$ is greater for the *P*/*M* interconversion of basket **1** in $CHCl_3$, $CFCl_3$ and $CCl_4$ (~2 kcal mol$^{-1}$ per solvent, Fig. 6C). Presumably, a considerable van der Waals steric strain is created in the operation of **1** as the guest (solvent) molecules press against the revolving pyridine gates. In contrast, more spacious and gated host **2** creates a sufficiently large aperture to permit in/out guest exchange and racemization with a smaller enthalpy of activation $\Delta H^{\ddagger}_{P/M}$ (Fig. 6C).

As noted in an earlier study,[30] the gates revolve at the basket's rim with and without in/out guest exchange; our experimental measurements, however, do not reveal the proportion of these two alternatives. In further discussion, we will therefore contemplate on the *P*/*M* racemization following $RM_{1-2}$ or $RM_3$ mechanisms with a guest (a) sitting inside baskets or (b) departing from their inner space (four mechanistic pathways).

In the case of the larger basket **2**, $CHCl_3/CH_2Cl_2/CFCl_3/CCl_4$ guests are too small to effectively populate its inner space (PC = 0.19–0.28) and affect the rotation of the pyridines at the rim. In this case, we presume that the preferred mechanism of

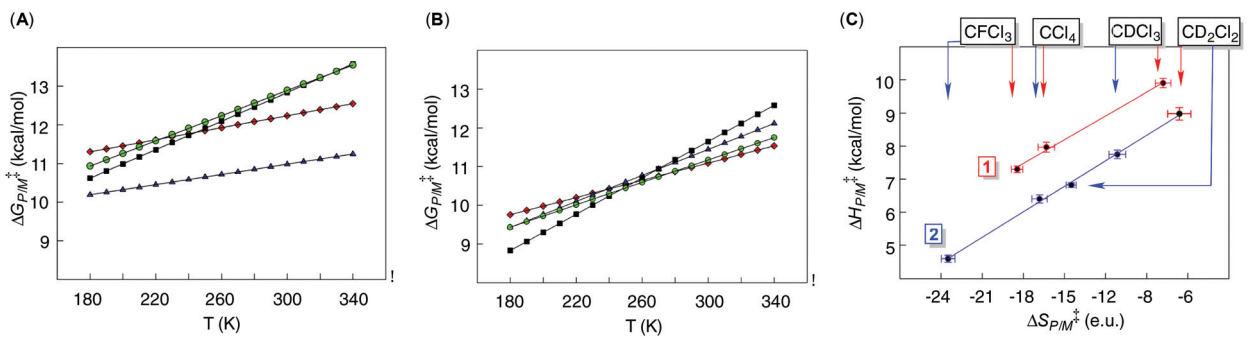


**Fig. 6** (A) The activation energy $\Delta G^{\ddagger}_{P/M}$ for the racemization of $\mathbf{1}_{P/M}$ in $CD_2Cl_2$ (blue), $CDCl_3$ (red), $CFCl_3$ (black, 30% $CD_2Cl_2$) and $CCl_4$ (green, 20% $CD_2Cl_2$) as a function of temperature. (B) The activation energy $\Delta G^{\ddagger}_{P/M}$ for the racemization of $\mathbf{2}_{P/M}$ in $CD_2Cl_2$ (blue), $CDCl_3$ (red), $CFCl_3$ (black, 30% $CD_2Cl_2$) and $CCl_4$ (green, 20% $CD_2Cl_2$) as a function of temperature; note that $\Delta G^{\ddagger}_{P/M}$ was calculated as $\Delta H^{\ddagger}_{P/M} - T\Delta S^{\ddagger}_{P/M}$ using data from Table 2. (C) The enthalpy/entropy compensation relationships ($R^2$ = 0.999, SigmaPlot) corresponding to the racemization of $\mathbf{1}_{P/M}$ (red) and $\mathbf{2}_{P/M}$ (blue) in four different solvents.

operation is $RM_{1-2}$ since it is easier to break two hydrogen bonds than three for opening the host; Table 3 shows that $RM_{1-2}$ dominates racemisations in the gas phase, yet our computations did not consider the swapping of entrapped guest with solvent molecule(s) and/or entropic changes in the process. When dichloromethane enters/exits basket **1**, a rather insignificant population of the basket's cavity (PC = 0.27) also enforces the $RM_{1-2}$ mechanistic pathway with only one pyridine gate opening to permit the racemization with/without the guest exchange.

For smaller basket **1** (226 Å$^3$), guests $CHCl_3$/$CFCl_3$/$CCl_4$ populate a greater portion of its cavity (PC = 0.33–0.39). The guest exchange would necessitate enough room, thereby enforcing the rotation of all three gates[28] and therefore the $RM_3$ mechanism. The sole *P*/*M* rotation of the gates, without the guest exchange, might perhaps follow the $RM_{1-2}$ alternative since it is energetically more favourable to break apart a single gate (Table 3). On the basis of our measurements (Fig. 6C), however, the guest exchange *via* the $RM_3$ mechanism must be dominating the racemisations with **1** carrying more sizeable guests.[28,30]

## Conclusions

Two differently sized baskets employ functionalized pyridine gates at the rim to form a seam of hydrogen bonds and thereby adopt *P* and *M* helical orientations. The *P*/*M* racemization mechanism appears to be a function of the guest's volume and could be elucidated by considering the population of the basket's cavity. Thus, larger guests that more efficiently fill the host (PC > 0.30) enforce the geared $RM_3$ pathway: the entrance/exit of guests necessitate the movement of all three gates. When the guest occupies a small portion of the inner space of the gated host (PC < 0.27), however, the rotation of one gate creates a large enough aperture for facile in/out guest exchange *via* the $RM_{1-2}$ mechanism.

Understanding the action of dynamic hosts, akin to **1** and **2**, is important for creating functional systems resembling those found in nature.[53] Our study about subtle mechanistic variations of molecular gating could be useful for improving catalysis[54] and/or controlling the trafficking of molecules in artificial environments.[55]

## Acknowledgements

This work was financially supported with funds obtained from the National Science Foundation (CHE-1012146, to J.D.B.) and the Department of Defense, the Defense Threat Reduction Agency (HDTRA1-11-1-0042, to J.D.B. and C.M.H.). The content of the information does not necessarily reflect the position or the policy of the federal government, and no official endorsement should be inferred. The Ohio Supercomputer Center is gratefully acknowledged for providing generous computational resources.

## Notes and references

1 D. J. Cram, *Nature*, 1992, **356**, 29–36.
2 F. Hof and J. Rebek Jr., *Proc. Natl. Acad. Sci. U. S. A.*, 2002, **99**, 4775–4777.
3 K. N. Houk, K. Nakamura, C. Sheu and A. E. Keating, *Science*, 1996, **273**, 627–629.
4 L. C. Palmer and J. Rebek Jr., *Org. Biomol. Chem.*, 2004, **2**, 3051–3059.
5 S. Rieth, K. Hermann, B.-Y. Wang and J. D. Badjic, *Chem. Soc. Rev.*, 2011, **40**, 1609–1622.
6 J. B. Wittenberg and L. Isaacs, *Supramol. Chem. Mol. Nanomater.*, 2012, **1**, 25–43.
7 R. G. Chapman, G. Olovsson, J. Trotter and J. C. Sherman, *J. Am. Chem. Soc.*, 1998, **120**, 6252–6260.
8 A. Varnek, S. Helissen, G. Wipff and A. Collet, *J. Comput. Chem.*, 1998, **19**, 820–832.
9 L. Garel, J. P. Dutasta and A. Collet, *Angew. Chem.*, 1993, **105**, 1249–1251 (*Angew. Chem., Int. Ed. Engl.*, 1993, **1232(1248)**, 1169–1271).
10 S. Mecozzi and J. Rebek Jr., *Chem.–Eur. J.*, 1998, **4**, 1016–1022.
11 J. Canceill, M. Cesario, A. Collet, J. Guilhem, L. Lacombe, B. Lozach and C. Pascard, *Angew. Chem.*, 1989, **101**, 1249–1251.
12 M. Rekharsky and Y. Inoue, *Supramol. Chem. Mol. Nanomater.*, 2012, **1**, 117–133.
13 C. A. Hunter, *Angew. Chem., Int. Ed.*, 2004, **43**, 5310–5324.
14 K. T. Chapman and W. C. Still, *J. Am. Chem. Soc.*, 1989, **111**, 3075–3077.
15 J. Canceill, L. Lacombe and A. Collet, *J. Am. Chem. Soc.*, 1986, **108**, 4230–4232.
16 A. Collet, *Compr. Supramol. Chem.*, 1996, **2**, 325–365.
17 N. R. Voss and M. Gerstein, *Nucleic Acids Res.*, 2010, **38**, W555–W562.
18 Z. Yan, T. McCracken, S. Xia, V. Maslak, J. Gallucci, C. M. Hadad and J. D. Badjic, *J. Org. Chem.*, 2008, **73**, 355–363.
19 A. Godec and F. Merzel, *J. Am. Chem. Soc.*, 2012, **134**, 17574–17581.
20 B. C. Gibb, *Chemosensors*, 2011, 3–18.
21 F. Hof, S. L. Craig, C. Nuckolls and J. Rebek Jr., *Angew. Chem., Int. Ed.*, 2002, **41**, 1488–1508.
22 I. A. Sedov, M. A. Stolov and B. N. Solomonov, *J. Phys. Org. Chem.*, 2011, **24**, 1088–1094.
23 N. Graulich, H. Hopf and P. R. Schreiner, *Chem. Soc. Rev.*, 2010, **39**, 1503–1512.
24 B.-Y. Wang, X. Bao, Z. Yan, V. Maslak, C. M. Hadad and J. D. Badjic, *J. Am. Chem. Soc.*, 2008, **130**, 15127–15133.
25 D. A. Evans and J. S. Evans, *J. Org. Chem.*, 1998, **63**, 8027–8030.
26 S. Tartaggia, A. Scarso, P. Padovan, O. De Lucchi and F. Fabris, *Org. Lett.*, 2009, **11**, 3926–3929.
27 B.-Y. Wang, X. Bao, S. Stojanovic, C. M. Hadad and J. D. Badjic, *Org. Lett.*, 2008, **10**, 5361–5364.

 

28 S. Rieth, X. Bao, B.-Y. Wang, C. M. Hadad and J. D. Badjic, *J. Am. Chem. Soc.*, 2010, **132**, 773–776.
29 B.-Y. Wang, S. Stojanovic, D. A. Turner, T. L. Young, C. M. Hadad and J. D. Badjic, *Chem.–Eur. J.*, 2013, **19**, 4767–4775.
30 K. Hermann, S. Rieth, H. A. Taha, B.-Y. Wang, C. M. Hadad and J. D. Badjic, *Beilstein J. Org. Chem.*, 2012, **8**, 90–99.
31 S. Rieth and J. D. Badjic, *Chem.–Eur. J.*, 2011, **17**, 2562–2565.
32 B.-Y. Wang, S. Rieth and J. D. Badjic, *J. Am. Chem. Soc.*, 2009, **131**, 7250–7252.
33 N. Bampos and A. Vidal-Ferran, *J. Chem. Educ.*, 2000, **77**, 130–133.
34 H. J. Reich, *J. Chem. Educ. Software, Ser. D*, 1996, **3D**, 17–19.
35 J. Svoboda, H. Schmaderer and B. Koenig, *Chem.–Eur. J.*, 2008, **14**, 1854–1865.
36 R. L. Williams and S. W. Shalaby, *J. Heterocycl. Chem.*, 1973, **10**, 891–899.
37 C. N. Eid Jr. and D. J. Cram, *J. Chem. Educ.*, 1993, **70**, 349–351.
38 B. C. Hamann, K. D. Shimizu and J. Rebek Jr., *Angew. Chem., Int. Ed. Engl.*, 1996, **35**, 1326–1329.
39 J. N. Israelachvili, *Intermolecular and Surface Forces*, 2011.
40 C. Valdes, L. M. Toledo, U. Spitz and J. Rebek Jr., *Chem.–Eur. J.*, 1996, **2**, 989–991.
41 R. Wyler, J. de Mendoza and J. Rebek Jr., *Angew. Chem.*, 1993, **105**, 1820–1821 (*Angew. Chem., Int. Ed. Engl.*, 1993, **1832(1812)**, 1699–1701).
42 R. Meissner, X. Garcias, S. Mecozzi and J. Rebek Jr., *J. Am. Chem. Soc.*, 1997, **119**, 77–85.
43 P. Timmerman, W. Verboom, F. C. J. M. van Veggel, J. P. M. van Duynhoven and D. N. Reinhoudt, *Angew. Chem.*, 1994, **106**, 2437–2440 (*Angew. Chem., Int. Ed. Engl.*, 1994, **2433(2422)**, 2345–2438).
44 R. G. Chapman, N. Chopra, E. D. Cochien and J. C. Sherman, *J. Am. Chem. Soc.*, 1994, **116**, 369–370.
45 A. Shivanyuk and J. Rebek, *Chem. Commun.*, 2002, 2326–2327.
46 K. Mislow, *Acc. Chem. Res.*, 1976, **9**, 26–33.
47 B. Laleu, G. Bernardinelli, R. Chauvin and J. Lacour, *J. Org. Chem.*, 2006, **71**, 7412–7416.
48 H. Ito, T. Abe and K. Saigo, *Angew. Chem., Int. Ed.*, 2011, **50**, 7144–7147.
49 S. Rieth, Z. Yan, S. Xia, M. Gardlik, A. Chow, G. Fraenkel, C. M. Hadad and J. D. Badjic, *J. Org. Chem.*, 2008, **73**, 5100–5109.
50 J. D. Dunitz, *Chem. Biol.*, 1995, **2**, 709–712.
51 W. Linert, *Chem. Soc. Rev.*, 1994, **23**, 429–438.
52 *Chemical Kinetics and Reaction Mechanisms*, ed. J. H. Espenson, 1995.
53 A. Gora, J. Brezovsky and J. Damborsky, *Chem. Rev.*, 2013, **113**, 5871–5923.
54 B.-Y. Wang, T. Zujovic, D. A. Turner, C. M. Hadad and J. D. Badjic, *J. Org. Chem.*, 2012, **77**, 2675–2688.
55 H.-X. Zhou and J. A. McCammon, *Trends Biochem. Sci.*, 2010, **35**, 179–185.